ELSEVIER

Materials Science and Engineering A268 (1999) 1–7

MATERIALS SCIENCE & ENGINEERING A

Analytical and numerical analyses for two-dimensional stress transfer

C.H. Hsueh [a,*], E.R. Fuller Jr. [b], S.A. Langer [b], W.C. Carter [b,1]

[a] *Oak Ridge National Laboratory, Oak Ridge, TN 37831-6068, USA*
[b] *National Institute of Standards and Technology, Gaithersburg, MD 20899, USA*

Received 7 December 1998; received in revised form 2 March 1999

Abstract

Both analytical modeling and numerical simulations were performed to analyze the stress transfer in platelet-reinforced composites in a two-dimensional sense. In the two-dimensional model, an embedded elongated plate bonded to a matrix along its long edges was considered. The system was subjected to both tensile loading parallel to the plate's long edges and residual thermal stresses. The ends of the plate can be debonded from or bonded to the matrix during loading, and both cases were considered in the analysis. Good agreement was obtained between the present analytical and numerical solutions. However, better agreement between analytical and numerical models was obtained for the case of bonded ends than for debonded ends. © 1999 Elsevier Science S.A. All rights reserved.

Keywords: Stress transfer; Interface; Composite; Analytical modeling; Numerical simulations

1. Introduction

Brittle ceramics can be reinforced by incorporating fibers [1,2], whiskers [3,4] or platelets [5–8]. The mechanics of reinforcement relies on stress transfer between the reinforced phase and the matrix, and analytical modeling has been developed to analyze this stress transfer. For fiber (and whisker) reinforcement, the shear lag model has been used extensively [9–15]. By treating fibers as ellipsoidal inclusions, the stress transfer problem has also been analyzed using both Eshelby's method for an ellipsoidal inclusion in an infinite matrix and the modification developed by Mori and Tanaka to account for the effect of finite volume fractions of inclusions [16,17]. For platelet reinforcement, a two-dimensional (plane stress) stress transfer model has also been developed [18,19]. To emphasize the two-dimensional nature of the analysis, 'plate' instead of 'platelet' is used hereafter. The initial two-dimensional stress transfer model [18] was derived by making the same assumptions and following the same analysis as used in the classical shear lag model [9]. The long edges of the elongated plate were assumed to be bonded to the matrix, and were parallel to the loading direction. The ends (i.e. short edges) of the plate were assumed to be debonded from the matrix such that stress transfer occurred only along the long edges of the plate [18]. Recently, a more rigorous two-dimensional stress transfer model was developed, and both cases of the plate-ends being debonded from and bonded to the matrix were considered [19]. However, residual thermal stresses were not included in the analysis. Also, a comparison between the analytical and numerical solutions has not been made.

The purpose of the present study was twofold. Firstly, the previous two-dimensional stress transfer analytical model [19] was modified to include residual thermal stresses. Secondly, numerical simulations were conducted on the two-dimensional stress transfer. Then, comparisons were made between analytical and numerical solutions.

2. Analytical modeling

The model composite for the two-dimensional stress transfer analysis is shown in Fig. 1. A plate with a

* Corresponding author. Tel.: +1-423-576-6568; fax: +1-423-574-8445.

[1] Present address: Massachusetts Institute of Technology, MA, USA.

0921-5093/99/$ - see front matter © 1999 Elsevier Science S.A. All rights reserved.
PII: S0921-5093(99)00129-X

width $2a$ and a length $2t$ is embedded at the center of a matrix with a width $2b$ and a length $2u$. The Cartesian coordinates, x and y, are also shown. A tensile stress, σ_o, is applied to the composite in the y-direction. The plate is bonded to the matrix at $x = \pm a$. At the ends of the plate (i.e. at $|x| \leq a$ and $y = \pm t$), the interfaces can either be debonded by mode I crack opening or remain bonded. Stresses transfer between the matrix and the plate through the interfacial shear stress, τ_i, at $x = \pm a$. In the case of bonded ends, stress transfer also occurs at $y = \pm t$. Due to the symmetric geometry in the x–y plane, only one quarter of the model composite is required in the analysis.

To simplify analyses in analytical modeling, the width of the plate was assumed to be much smaller than that of the matrix. Hence, whereas the x-dependence of the stress, σ_y, was considered in the matrix, it was ignored in the plate [19]. For convenience, σ_y is designated as σ_p and σ_m for the plate and the matrix, respectively. The general differential equation governing the stress distribution in the plate along the y-direction, σ_p, due to stress transfer has been derived, such that [19]

$$\frac{d^2\sigma_p}{dy^2} = \frac{3[a\sigma_p - b\sigma_o + (b-a)\sigma_a]}{2a(b\text{-}a)^2(1+\nu_m)} \tag{1}$$

where ν_m is Poisson's ratio of the matrix, and σ_a is the matrix stress in the y-direction at the interface (i.e. σ_m at $x = a$). The interfacial shear stress, τ_i, is related to σ_p by [19]

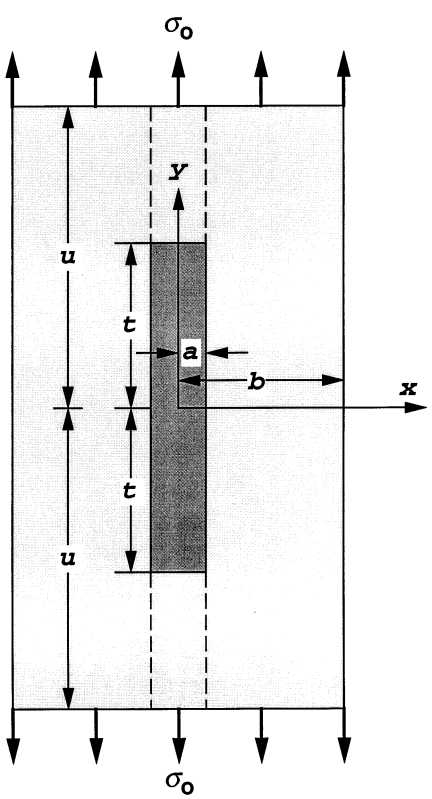

Fig. 1. Schematic showing the two-dimensional stress transfer model.

$$\tau_i = -\frac{ad\sigma_p}{dy} \tag{2}$$

The general solution of σ_p from Eq. (1) is contingent upon the determination of σ_a.

The role of Poisson's effect in analyzing the stress transfer problem has been addressed previously [20,21]. While Poisson's effect is important when the interface is debonded and subjected to Coulomb friction [20], the error resulting from ignoring Poisson's effect is negligible when the interface is bonded [21]. The strain in the system consists of the thermal strain (which is a stress-free strain) and the stress-induced strain. The condition that the plate and the matrix remain bonded at the interface requires continuity of the strain in the y-direction. Ignoring Poisson's effect, this condition is described by

$$\alpha_p \Delta T + \frac{\sigma_p}{E_p} = \alpha_m \Delta T + \frac{\sigma_a}{E_m} \quad (\text{at } x = a) \tag{3}$$

where E and α are Young's modulus and the coefficient of thermal expansion, the subscripts p and m denote the plate and the matrix, respectively, and ΔT is the temperature change for thermal stress development.

Substituting Eq. (3) into Eq. (1), the general solution for σ_p is

$$\sigma_p = \frac{bE_p\sigma_o - (b-a)E_pE_m(\alpha_p - \alpha_m)\Delta T}{aE_p + (b-a)E_m} + A\exp(\beta y) + B\exp(-\beta y) \quad (\text{for } 0 \leq y \leq t) \tag{4}$$

where

$$\beta = \frac{1}{b-a}\left\{\frac{3[aE_p + (b-a)E_m]}{2a(1+\nu_m)E_p}\right\}^{1/2} \tag{5}$$

The corresponding interfacial shear stress, τ_i, is

$$\tau_i = -a\beta[A\exp(\beta y) - B\exp(-\beta y)] \quad (\text{for } 0 \leq y \leq t) \tag{6}$$

Determination of the coefficients, A and B, is contingent upon the boundary condition at the plate-ends.

2.1. The bonded-ends case

When the ends of the plate are bonded to the matrix, stress transfer occurs such that a finite stress exists at the bonded ends. The boundary condition at the bonded ends is defined by the continuity condition at $y = \pm t$. To satisfy this continuity condition, a technique of adding imaginary plates to the stress transfer model has been developed [19]. The matrix connecting the plate ends to the surface (see the area, $|x| \leq a$ and $|y| \geq t$, between dashed-lines in Fig. 1) is treated as two imaginary plates, which have the matrix properties.

Whereas the general solutions of σ_p and τ_i in the real plate are described respectively by Eq. (4) and Eq. (6), the general solutions of the stress in the y-direction, σ'_p,

and the interfacial shear stress, τ_i', for the imaginary plate can be obtained by letting $\alpha_p = \alpha_m$ and $E_p = E_m$ in Eq. (4), Eq. (5) and Eq. (6), such that

$$\sigma_p' = \sigma_o + A'\exp(\beta' y) + B'\exp(-\beta' y) \quad (\text{for } t \le y \le u) \tag{7}$$

$$\tau_i' = -a\beta'[A'\exp(\beta' y) - B'\exp(-\beta' y)] \quad (\text{for } t \le y \le u) \tag{8}$$

where

$$\beta' = \frac{1}{b-a}\left[\frac{3b}{2a(1+\nu_m)}\right]^{1/2} \tag{9}$$

To solve the coefficients, A and B for the real plate and A' and B' for the imaginary plate, four boundary conditions are required which are

$$\sigma_p' = \sigma_o \quad (\text{at } y = u) \tag{10a}$$

$$\sigma_p = \sigma_p' \quad (\text{at } y = t) \tag{10b}$$

$$\tau_i = \tau_i' \quad (\text{at } y = t) \tag{10c}$$

$$\tau_i = 0 \quad (\text{at } y = 0) \tag{10d}$$

Eq. (10a) is the loading condition, Eq. (10b) and Eq. (10c) are the continuity conditions, and Eq. (10d) is the symmetry condition.

The solutions of A, B, A', and B' subjected to the above boundary conditions are

$$A = \frac{(b-a)(E_m - E_p)\sigma_o + (b-a)E_pE_m(\alpha_p - \alpha_m)\Delta T}{aE_p + (b-a)E_m} \times \left\{\exp(\beta t) + \exp(-\beta t) - \frac{\beta[\exp(\beta t) - \exp(-\beta t)][\exp(\beta' t) - \exp(2\beta' u - \beta' t)]\beta'[\exp(\beta' t) + \exp(2\beta' u - \beta' t)]}{}\right\}^{-1} \tag{11a}$$

$$B = A \tag{11b}$$

$$A' = \frac{\beta[\exp(\beta t) - \exp(-\beta t)]A}{\beta'[\exp(\beta' t) + \exp(2\beta' u - \beta' t)]} \tag{11c}$$

$$B' = -A'\exp(2\beta' u) \tag{11d}$$

The solutions for the bonded-end case are hence completed.

When the bonded end is sufficiently remote from the loading surface such that $\exp(2\beta' u) >> \exp(\beta' t)$, the coefficient A $(=B)$ can be simplified, and σ_p at the bonded end has an asymptotic value; i.e.

$$\sigma_p = \frac{\sigma_o}{aE_p + (b-a)E_m}\left\{bE_p + \frac{(b-a)\beta'(E_m - E_p)[\exp(\beta t) + \exp(-\beta t)]}{\beta'[\exp(\beta t) + \exp(-\beta t)] + \beta[\exp(\beta t) - \exp(-\beta t)]}\right\} + \frac{(b-a)E_pE_m(\alpha_p - \alpha_m)\Delta T}{aE_p + (b-a)E_m}\left\{-1 + \frac{\beta'[\exp(\beta t) + \exp(-\beta t)]}{\beta'[\exp(\beta t) + \exp(-\beta t)] + \beta[\exp(\beta t) - \exp(-\beta t)]}\right\} \quad (\text{at } y = t \text{ and for } u - t >> 0) \tag{12}$$

When the plate is sufficiently long such that $\exp(\beta t) >> 0 >> \exp(-\beta t)$, the coefficient A $(=B)$ can also be simplified, and σ_p in the central region of the plate reaches its asymptotic value; i.e.

$$\sigma_p = \frac{bE_p\sigma_o - (b-a)E_pE_m(\alpha_p - \alpha_m)\Delta T}{aE_p + (b-a)E_m} \quad (\text{at } y = 0 \text{ and for } t >> 0) \tag{13}$$

Alternatively, the asymptotic value of the stress in the plate (Eq. (13)) can also be derived from a simple equilibrium equation; i.e. the stresses in the plate and the matrix, σ_p and σ_m, are uniform and reach their asymptotic values at y-positions sufficiently remote from the plate end, and

$$a\sigma_p + (b-a)\sigma_m = b\sigma_o \tag{14}$$

Also, continuity at the interface requires that

$$\alpha_p\Delta T + \frac{\sigma_p}{E_p} = \alpha_m\Delta T + \frac{\sigma_m}{E_m} \tag{15}$$

Combination of Eq. (14) and Eq. (15) yields Eq. (13).

2.2. The debonded-ends case

When the ends of the plate are debonded from the matrix, stresses cannot be transferred through the ends (i.e. $\sigma_p = 0$ at $y = t$), and the symmetric geometry requires that $\tau_i = 0$ at $y = 0$. The solutions of σ_p and τ_i from Eq. (4) and Eq. (6) subjected to the above two boundary conditions are

$$\sigma_p = \frac{bE_p\sigma_o - (b-a)E_pE_m(\alpha_p - \alpha_m)\Delta T}{aE_p + (b-a)E_m}\left[1 - \frac{\exp(\beta y) + \exp(-\beta y)}{\exp(\beta t) + \exp(-\beta t)}\right] \quad (\text{for } 0 \le y \le t) \tag{16}$$

$$\tau_i = \frac{a\beta[bE_p\sigma_o - (b-a)E_pE_m(\alpha_p - \alpha_m)\Delta T]}{aE_p + (b-a)E_m}\left[\frac{\exp(\beta y) - \exp(-\beta y)}{\exp(\beta t) + \exp(-\beta t)}\right] \quad (\text{for } 0 \le y \le t) \tag{17}$$

It is noted that σ_p described by Eq. (16) also approaches Eq. (13) at $y = 0$ when $t >> 0$.

For the imaginary plate, $\sigma'_p = 0$ at $y = t$ because of the debonded end, and the loading condition requires that $\sigma'_p = \sigma_o$ at $y = u$. The solutions of σ'_p and τ'_i from Eq. (7) and Eq. (8) subjected to the above two boundary conditions are

$$\sigma'_p = \sigma_o\left[1 - \frac{\exp(\beta' y) - \exp(2\beta' u - \beta' y)}{\exp(\beta' t) - \exp(2\beta' u - \beta' t)}\right] \quad (\text{for } t \le y \le u) \tag{18}$$

$$\tau'_i = a\beta'\sigma_o\left[\frac{\exp(\beta' y) + \exp(2\beta' u - \beta' y)}{\exp(\beta' t) - \exp(2\beta' u - \beta' t)}\right] \quad (\text{for } t \le y \le u) \tag{19}$$

3. Numerical simulations

Both a recently developed object oriented finite element analysis (OOF) [22] and a conventional finite element code, ANSYS 5.4 [23], were adopted for numerical simulations. Due to the symmetric geometry depicted in Fig. 1, only one quarter of the geometry ($0 \le x \le b$ and $0 \le y \le u$) is required for the simulations. The boundary conditions require fixing both the x-displacement at $x = 0$ and the y-displacement at $y = 0$. Loading is applied at $y = u$.

3.1. OOF

For OOF, a two-dimensional uniform grid was used and each grid consisted of two triangular elements. The region of $0 \le x \le b$ and $0 \le y \le u$ in Fig. 1 was digitized to a portable pixel map (*.ppm*) format; each pixel then corresponding to two triangular elements. Hence, meshing in OOF is obtained simply by converting an image to a portable pixel map format. The uniqueness of OOF is that it can operate directly on microstructural images. However, to achieve high accuracy in the simulated results, many more elements are required in OOF than in conventional finite element programs (e.g. ANSYS). It is noted that loading in OOF is via forces applied at nodes. To achieve uniform loading stress, the force applied at the two corner-nodes (i.e. at $(x, y) = (0, u)$ and (b, u) in Fig. 2a) should be half of the force applied at other nodes.

3.2. ANSYS

For ANSYS, a two-dimensional quadratic, structural, higher-order eight-node element, PLANE82, was used in the present study. Meshing was obtained by using automatic meshing and followed by refinements of the elements in the plate-end region. Loading in ANSYS is via a pressure applied at the element boundary line.

4. Comparison

In order to make the comparison between analytical and numerical solutions, $b/a = 10$, $t/a = 15$, $u/a = 30$, $E_p = 300$ GPa, $E_m = 100$ GPa, $\nu_p = 0.3$, $\nu_m = 0.3$, $\sigma_o = 100$ MPa, $\alpha_p = 3 \times 10^{-6}/^{o}C$, $\alpha_m = 4 \times 10^{-6}/^{o}C$, and $\Delta T = -1000^{o}C$ were used in the present study. For OOF, the digitized image for numerical simulations consisted of 54 200 elements. For ANSYS, the mesh containing 268 elements (865 nodes for bonded ends and 877 nodes for debonded ends) is shown in Fig. 2a while the details in the plate-end region are shown in Fig. 2b. While the x-dependence of σ_p (and σ'_p) was ignored in analytical modeling, the solutions for σ_p (and σ'_p) from numerical simulations were averaged with respect to $0 \le x \le a$ to compare with analytical solutions. The distributions of the stress in the loading direction, σ_p and σ'_p, are shown in Fig. 3 and Fig. 4 for the cases of bonded-ends and debonded-ends, respectively. The boundary between the imaginary and the real plates (i.e. the position of the plate-end) as well as the asymptotic stresses in the plate at $y = 0$ (Eq. (13)) are also shown. With the dimension shown in Fig. 2, the plate-end is sufficiently remote from the loading surface, and the analytical solution for σ_p at the plate-end, $y = t$, reaches its asymptotic value described by Eq. (12).

4.1. The bonded-ends case

For the bonded-ends case, the solutions for loading only, residual thermal stresses only, and combined loading/thermal stresses are shown. While the analytical solutions are shown in both Fig. 3a and Fig. 3b, the OOF and ANSYS results are shown in Fig. 3a and Fig. 3b, respectively. Excellent agreement between analytical and numerical solutions is obtained, and the following results can be concluded. Firstly, the stress at $y = u$ is σ_o or zero depending upon whether a load is applied. The stress transfers between the matrix and the imaginary plate because of the existence of the real plate underneath. Secondly, at the boundary between the imaginary and the real plates (i.e. at the plate-end, $y = t$), the stress has a finite value. This finite value has an asymptotic value described by Eq. (12) when the loading surface is sufficiently remote from the plate end. Thirdly, the stress continuously transfers between the matrix and the real plate. The stress in the real plate reaches an asymptotic value described by Eq. (13) when the plate is sufficiently long.

4.2. The debonded-ends case

For the debonded-ends case, the solutions for loading only and combined loading/thermal stresses are shown. The solutions for thermal stresses only are not

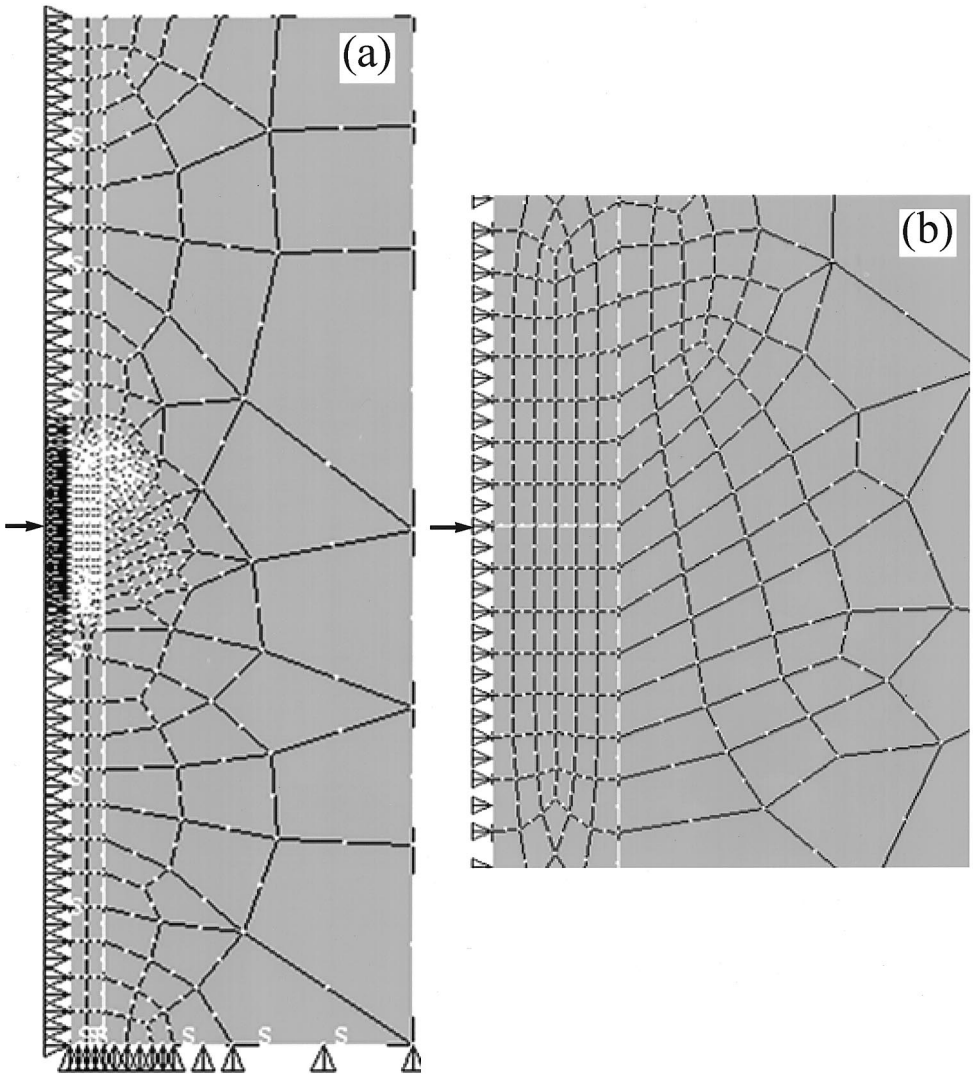

Fig. 2. The finite element mesh used in ANSYS for two-dimensional stress transfer analyses showing (a) quarter of the model composite depicted by Fig. 1, and (b) details in the plate-end region. The plate-end position is indicated by an arrow.

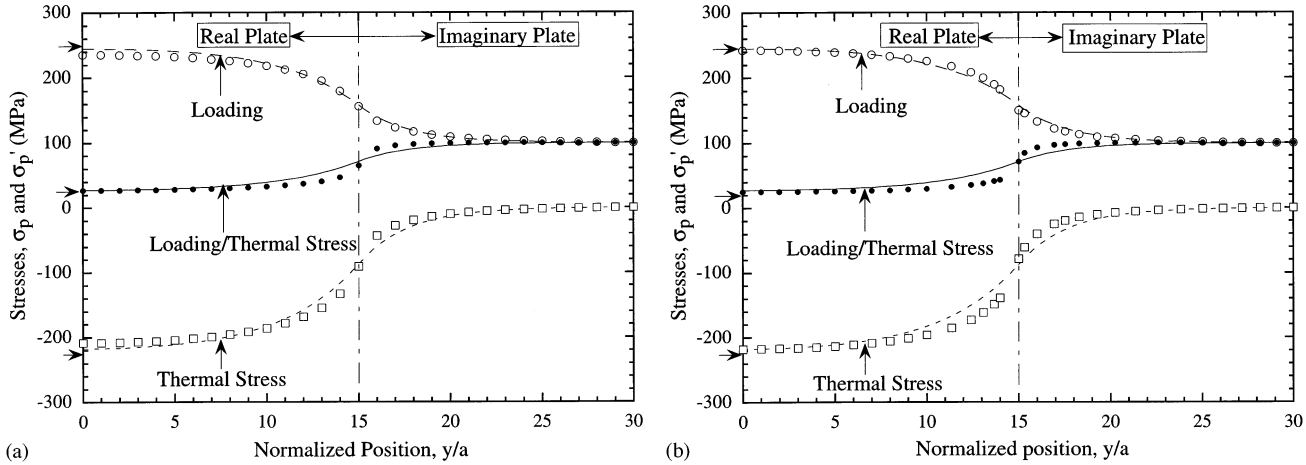

Fig. 3. The stress distribution, σ_p and σ'_p, along the real and the imaginary plates for the bonded-ends case. (a) Analytical and OOF solutions, and (b) analytical and ANSYS solutions for loading only, residual thermal stresses only, and combined loading/thermal stresses. (lines: analytical solutions; symbols: numerical solutions; arrows at $y = 0$: asymptotic values).

shown because the plate-ends are under residual compression, and the free-ends condition is not satisfied. While the analytical solutions are shown in both Fig. 4a and Fig. 4b, the OOF and ANSYS results are shown in Fig. 4a and Fig. 4b, respectively. For the imaginary plate, the analytical solution of σ'_p shows no dependence on the residual thermal stresses (see Eq. (18)). Hence, the analytical solutions of σ'_p for loading only and for combined loading/thermal stresses overlap in Fig. 4. For OOF, empty elements are used to simulate the debonded end, and $\sigma_p = 0$ at the debonded end (see Fig. 4a). For ANSYS, two sets of nodes are assigned at the debonded end with a merged node at $(x,y) = (a,t)$ allowing a crack to open at the debonded end when it is subjected to tension. As a result, two solutions are obtained for σ_p at the debonded end. Also, since stresses are derived from the displacement solutions in ANSYS and the nodal solution of stress is obtained by averaging the element values at the shared node, non-zero values (but small magnitudes) of σ_p are shown at the debonded end (see Fig. 4b).

It is noted that excellent agreement is obtained between the two numerical solutions, OOF and ANSYS. It is also noted that the agreement between the analytical and the numerical solutions for the debonded-ends case is not as good as that for the bonded-ends case, especially in the region of the plate-ends. This lack of agreement probably results from the complicated singularity [24] which occurs at $y = t$ in this case. The analytical approach based on the shear lag model is unable to directly handle this singularity. The numerical approach, if meshed using the singular element around the crack tip, can approximate the steep stress gradients near the plate-ends. However, the difference in ANSYS results between using quadratic element with refinements of elements in the plate-end region (see Fig. 2) and adding the singular element is negligible. This can be due to the fact that the numerical results of interest are σ_p (and σ'_p) averaged with respect to $0 \le x \le a$ (not the stress intensity factor) to compare with analytical solutions. Hence, the difference between the analytical and the numerical solutions for the debonded-ends case is mainly due to the inability of analytical modeling in handling the singularity problem. Nonetheless, the analytical solutions derived in the present study provide a simple closed-form approximation that is not radically incorrect.

5. Concluding remarks

Whereas the analytical stress transfer model has been well established for fiber-reinforced composites, its use for platelet-reinforced composites has not been developed to the same extent. Analytical solutions for two-dimensional stress transfer are provided in the present study to simulate stress transfer in platelet-reinforced composites. In the paucity of existing theoretical analyses and experimental measurements for the stress transfer phenomena in platelet-reinforced composites, two-dimensional numerical simulations were also performed in the present study to verify the present analytical solutions. The present analytical solutions provide a basis in analyzing stress transfer in platelet-reinforced composites. However, they are two-dimensional and are, hence, preliminary. A more comprehensive model is hoped to emerge in the future by considering the three-dimensional nature of platelet-reinforced composites.

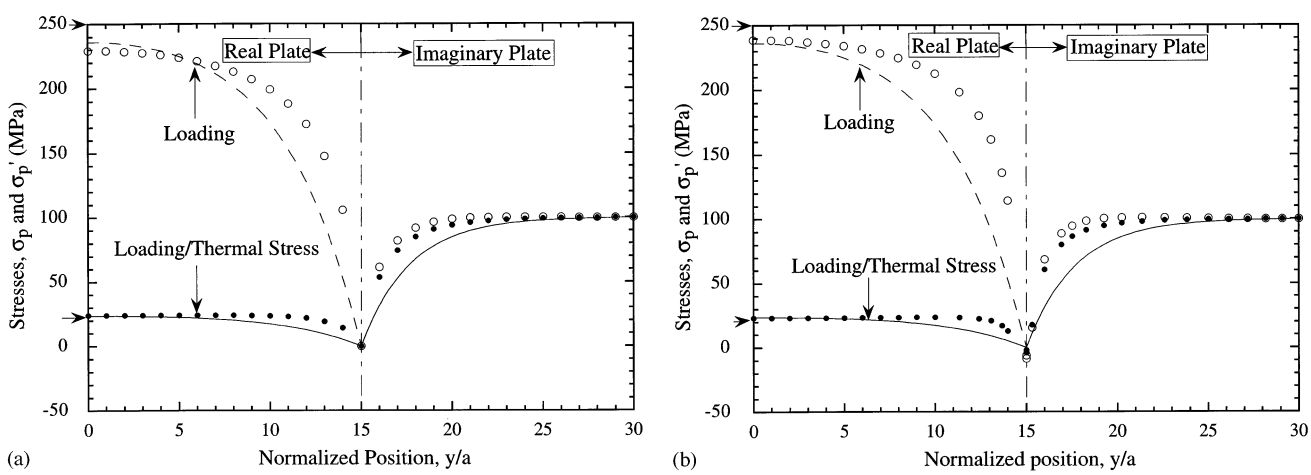

Fig. 4. The stress distribution, σ_p and σ'_p, along the real and the imaginary plates for the debonded-ends case. (a) Analytical and OOF solutions, and (b) analytical and ANSYS solutions for loading only, and combined loading/thermal stresses. (lines: analytical solutions; symbols: numerical solutions; arrows at $y = 0$: asymptotic values).

Acknowledgements

The authors thank Dr T.J. Chuang for running ANSYS with singular elements, and Drs P.F. Becher, M.J. Andrews, E.Y. Sun, and R.B. Clough for reviewing the manuscript. CHH acknowledges support of the US Department of Energy, Division of Materials Sciences, Office of Basic Energy Sciences, under contract DE-AC05-96OR22464 with Lockheed Martin Energy Research Corp. ERF acknowledges support of the Alexander von Humboldt Foundation.

References

[1] J.J. Brennan, K.M. Prewo, J. Mater. Sci. 17 (1982) 2371–2383.
[2] H. Kodama, H. Sakamoto, T. Miyoshi, J. Am. Ceram. Soc. 72 (4) (1989) 551–558.
[3] P.F. Becher, G.C. Wei, J. Am. Ceram. Soc. 67 (12) (1984) C267–C269.
[4] K. Jakus, S.V. Nair, Ceram. Eng. Sci. Proc. 9 (7-8) (1988) 767–776.
[5] M.R. Piggott, Load Bearing Fiber Composites, Pergamon Press, Elmsford, NY, 1980, p. 141.
[6] K.H. Heussner, N. Claussen, J. Euro. Ceram. Soc. 5 (1989) 193–200.
[7] D. Baril, M.K. Jain, Ceram. Eng. Sci. Proc. 12 (7-8) (1991) 1175–1192.
[8] Y.S. Chou, D.J. Green, J. Am. Ceram. Soc. 76 (6) (1993) 1452–1458.
[9] H.L. Cox, Br. J. Appl. Phys. 3 (1952) 72–79.
[10] P. Lawrence, J. Mater. Sci. 7 (1) (1972) 1–6.
[11] A. Takaku, R.G.C. Arridge, J. Phys. D: Appl. Phys. 6 (1973) 2038–2047.
[12] Y.C. Gao, Y.W. Mai, B. Cotterell, J. Appl. Math. and Phys. (ZAMP) 39 (7) (1988) 550–572.
[13] B. Budiansky, J.W. Hutchinson, A.G. Evans, J. Mech. Phys. Solids 34 (2) (1986) 167–189.
[14] C.H. Hsueh, J. Mater. Sci. Lett. 7 (5) (1988) 497–500.
[15] C.H. Hsueh, Mater. Sci. Eng. A125 (1) (1990) 67–73.
[16] C.H. Hsueh, J. Am. Ceram. Soc. 72 (2) (1989) 344–347.
[17] C.H. Hsueh, P.F. Becher, Mater. Sci. Eng. A212 (1996) 22–28.
[18] W.R. Tyson, G.J. Davies, Br. J. Appl. Phys. 16 (1965) 199–205.
[19] C.H. Hsueh, Compos. Eng. 4 (10) (1994) 1033–1043.
[20] C.H. Hsueh, J. Mater. Sci. Lett. 8 (1989) 739–742.
[21] C.H. Hsueh, J. Mater. Sci. Lett. 10 (1991) 29–32.
[22] S.A. Langer, W.C. Carter, E.R. Fuller, Object Oriented Finite Element Analysis for Materials Science, Center for Theoretical and Computational Materials Science and the Information Technology Laboratory at the National Institute of Standards and Technology, 1997.
[23] ANSYS Release 5.4, SAS IP, Inc., Houston, PA (1997).
[24] Y. Weitsman, H. Zhu, J. Mech. Phys. Solids 41 (2) (1993) 351–388.